Springer

KSME

Journal of Mechanical Science and Technology 26 (2) (2012) 463~471
www.springerlink.com/content/1738-494x
DOI 10.1007/s12206-011-1210-5

Reconstruction of time-domain impedance boundary condition considering the incident intensity effect on perforated-plate acoustic liner †

Minwoo Kim[1], Jonghoon Bin[2] and Soogab Lee[1,3,*]

[1]*School of Mechanical and Aerospace Engineering, Seoul National University, Seoul, 151-742, Korea*
[2]*Computational Science and Engineering, Florida State University, MCH 413, Tallahassee, FL 32306-4510, United States*
[3]*Engineering Research Institute, Seoul National University, Seoul, 151-742, Korea*

(Manuscript Received March 19, 2011; Revised September 26, 2011; Accepted September 29, 2011)

Abstract

Based on impedance prediction methods for a perforated plate acoustic liner, time-domain impedance boundary conditions are enhanced with consideration of incident intensity. The impedance coefficient of the time-domain boundary condition is re-derived using parameters of the liner structure, and is classified by physical characteristics. To show the capability of the reconstructed impedance boundary condition, two numerical calculations are performed with comparison to analytical results. The first considers the one-dimensional wave propagation problem to account for the reflection wave due to an incident intensity variation on the acoustic liner. The second considers the excess attenuation of impedance surface. The numerical simulation is performed using the linearized Euler equations (LEEs). Dispersion-relation-preserving finite difference scheme and optimized Adams-Bashforth time-integration method are used spatial discretization / time integration, respectively. The numerical results show excellent agreement with analytical results. Moreover, a reconstruction method of impedance boundary condition can easily obtain the impedance coefficients under environments of variant magnitudes of incident waves.

Keywords: Acoustic liner; Computational aeroacoustics; Impedance boundary condition

1. Introduction

Acoustic liners have been widely used in the aeroacoustic noise reduction such as engine fan noise. Acoustic liner consists of perforated panel and honeycomb-type cells. Cavities of honeycomb-type cells and pores of perforated panels cause the acoustic liner to behave as a Helmholtz resonator [1-3]. The acoustic behaviors of acoustic liner can be characterized by acoustic impedance. Impedance is defined as the ratio of the acoustic pressure to the acoustic velocity normal to the surface of acoustic liner.

$$p(\vec{x},\omega) = Z(\omega) v_n(\vec{x},\omega) \tag{1}$$

$$Z = R - iX \tag{2}$$

where Z represents the surface impedance of the acoustic liner with complex variable with R and X. p and v_n represent the acoustic pressure and particle velocity in the frequency domain (they generally have the time dependence with $e^{-i\omega t}$).

In aeroacoustic calculation, impedance surface is considered as absorbing boundary condition. Tam initiated the stable time-domain impedance boundary condition for computational Aeroacoustics (CAA) [4]. Tam derived impedance formula with three impedance parameters. Özyörük suggested complicated impedance model using z-transform method [5]. Rienstra proposed an Extended Helmholtz Resonator (EHR) type impedance model [6]. Fung and Ju proposed effective reflection wave modeling [7]. Bin and Hussaini proposed a second order frequency response function model [8]. The numerical result of time-domain impedance boundary conditions (TDIBCs) shows good agreement with the analytical solutions. Moreover, TDIBC guarantees the numerical stability for time-domain calculation. However, nonlinear effect due to the high sound pressure level (SPL) is not considered in time-domain impedance boundary conditions [9]. TDIBCs are derived by the impedance experimental data with same incident SPL. In this reasons, TDIBC is valid on the same incident pressure magnitude, which means that impedance models do not ensure the reliability for the arbitrary incident pressure.

The objective of this paper is to expand time-domain impedance boundary conditions for all incident sound pressure

† This paper was recommended for publication in revised form by Associate Editor Dongshin Shin

* Corresponding author. Tel.: +82 2 880 7384, Fax.: +82 2 876 4360
E-mail address: solee@snu.ac.kr

level. For perforated-plate acoustic liner, GE prediction model is chosen for impedance prediction model. Impedance prediction model is categorized by function of incident wave term. Impedance prediction model is modified into TDIBC form using simple approximation. GE impedance prediction model is re-written as time-domain impedance models. For time-domain computation, incident sound pressure level is accounted by incident particle velocity on impedance surface. TDIBC coefficients are reconstructed using a function of incident wave. In this paper, we choose the 6.7%-perforated acoustic liner for sample impedance material. We derive the TDIBC coefficients with incident wave and apply the numerical boundary condition. In order to show the incident wave effect on boundary condition, two types of numerical investigation are performed and are compared with analytical results. First, we consider a one-dimensional (1-D) wave propagation problem to account for the reflection wave due to variation of incident intensity on the acoustic liner. Second, we evaluate the excess attenuation of impedance surface under conditions of variant quasi-broadband acoustic sources.

The paper is organized as follows. Section 2 describes the impedance prediction models and time-domain impedance model. Section 3 discusses the re-construction method that uses coupling of the impedance prediction model and the time-domain impedance model. Section 4 presents the numerical investigations of the re-constructed boundary condition. Concluding remarks are mentioned in Section 5.

2. Impedance model

2.1 Brief review of broadband impedance model

The characteristic of acoustic impedance is usually described in the frequency-domain by assuming that the variation in magnitude of the incident acoustic pressure is negligible. The impedance quantity in the frequency-domain has the specified complex value described in Eq. (2). In a broadband condition, however, a proper treatment of an impedance model is required for a time-domain numerical simulation. In this paper, three kinds of broadband impedance models are considered as base impedance boundary condition for re-construction.

The first model is a mechanical impedance model proposed by Tam and Auriault [4]. They suggested that broadband impedance model is a form of impedance of electric circuits or mechanical systems. An acoustic liner system with a single degree-of-freedom is modeled as mass-spring-damper system. The normalized impedance can be expressed as

$$\frac{Z}{\rho_0 c_0} = R_0 - i\left(X_+\omega + X_-\omega^{-1}\right) \tag{3}$$

where ω is the angular frequency and i is the imaginary number $\sqrt{-1}$. The coefficients R_0, X_+, and X_- are the resistance and reactance quantities. The impedance model is constructed by regression method of impedance experimental data. A variation in resistance value is much smaller than that of the reactance in the frequency-domain, thus, the resistance coefficient R_0 is considered to be a constant value.

The second broadband impedance model is an extended Helmholtz resonator (EHR) model proposed by Rienstra [6]. EHR model is based on mechanical impedance model and is constructed by using resonance frequency of Helmholtz resonator. Basic form of EHR model is similar with three parameter impedance model. Frequency dependency term R_f is added on EHR model:

$$\frac{Z}{\rho_0 c_0} = R_0 + R_f + (-i\omega)X_+ + (-i\omega)^{-1}X_- . \tag{4}$$

All impedance coefficients are derived by resonance frequency of Helmholtz resonator and geometric parameters of Helmholtz resonator. Resistance terms should be even functions to satisfy time-domain stability, and reactance terms should be odd functions by stability condition.

The third broadband impedance model is a second-order frequency response function (FRF) model proposed by J. Bin et al. [8]. A second-order FRF model is designed to limit the order of the impedance model. When the broadband impedance function from experimental data is complicated, the order of the impedance model increases. The order due to the complicated impedance model leads to difficulties in the time-domain treatment of impedance model. To avoid such difficulties, a broadband impedance model can be divided into several second-order FRFs as following form:

$$\frac{Z}{\rho_0 c_0} = \sum_{j=1}^{N} \frac{a_0^j(-i\omega) + a_1^j}{b_0^j(-i\omega)^2 + b_1^j(-i\omega) + b_2^j} \tag{5}$$

where the variables series of a and b are the positive values. The maximum order of the impedance model is limited to one or two.

All the time-domain impedance models take a polynomial form of $-i\omega$. The even polynomials represent resistance of impedance and the odd polynomials represent reactance impedance. The complex variable $-i\omega$ is replaced with the partial derivative with respect to time $\partial/\partial t$ by consideration of the harmonic wave assumption, $e^{-i\omega t}$. In this paper, we take three parameter impedance model.

2.2 Impedance prediction method of perforated-plate acoustic liner

Mostinger and Kraft suggested an impedance prediction model for perforated-plate acoustic liner [10]. GE impedance prediction model consist with the geometric parameters of perforated plate and incident intensity. The geometric parameters are shown in Fig. 1.

For GE impedance prediction model [10], the normalized impedance formula consists of slope function of magnitude of incident wave U and independent variable with respect to

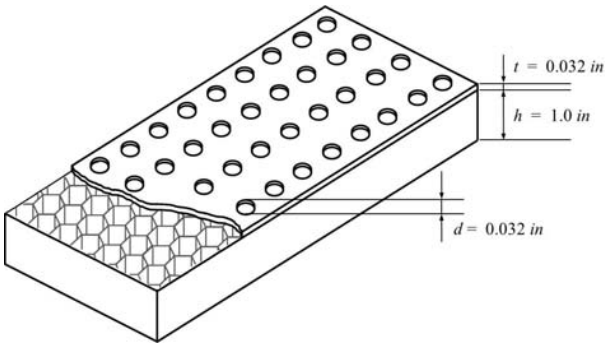

Fig. 1. Geometric parameters of a perforated-panel [1].

incident wave U .

$$\frac{Z}{\rho_0 c_0} = R_{GE} + f_R(U) - i\left[X_m - f_x(U) - \cot(kh)\right] \tag{6}$$

Independent variables R_{GE} and X_m are defined as follows:

$$R_{GE} = \frac{32\mu t}{\rho_0 c_0 C_D d^2}, \quad X_m = \frac{k(t+\varepsilon d)}{\sigma}. \tag{7a}$$

Slope functions $f_R(U)$ and $f_X(U)$ are defined as follows:

$$f_R(U) = \left[1.3365451\frac{1}{2c_0}\frac{1-\sigma^2}{(\sigma C_D)^2}\right]\cdot U,$$
$$f_X(U) = \left[0.119\frac{k}{\sigma}d\right]\cdot \log(U) \tag{7b}$$

where ρ_0 is density of air, c_0 is speed of sound and μ is viscosity of air for air conditions. d is diameter of pore, t is thickness of faceplate, h is depth of cells and σ is porosity which is defined as $\sigma = n(\pi d^2)/4S$ (n is number of pores and S is area of faceplate) for liner geometric parameters. ε is end-correction factor and C_D is discharging coefficients from orifice theory. Slope function $f_X(U)$ is valid on the range of $0 \le U \le 4.93$ (m/s) [10, 11].

According to the impedance prediction model, a resistance term is a function with respect to the incident wave. Likewise, a reactance term consists of a function of incident wave and a cavity reactance. The impedance quantities are determined by the conditions of the acoustic liner and incident intensity.

3. Reconstruction of impedance boundary condition

3.1 Treatment of impedance boundary condition.

The time-domain impedance models described in Eq. (3) indicate the variation of impedance value in frequency-domain. In addition, the impedance prediction model which is described in Eqs. (6) and (7) indicates the dependence of the incident acoustic velocity. To combine the variation in frequency domain, linear dependency of acoustic velocity incident, the impedance prediction model of Eq. (6) would be changed into a form of Eq. (3)

From impedance prediction model from Eq. (6), normalized resistance can be obtained as follows:

$$\frac{R}{\rho_0 c_0} = R_{GE} + f_R(U).$$

The resistance can be divided into an initial resistance R_{GE} and a slope function $f_R(U)$. The initial R_{GE} might be a constant or arbitrary function with respect to ω based on the prediction method. If R_{GE} is constant, the time-domain impedance model is a simple impedance model. Otherwise, time-domain impedance model must be a form of EHR or FRF impedance model. The incident term $f_R(U)$ is independent of frequency variation. Hence, resistance R can be determined by the GE impedance prediction model.

From the reactance from the impedance prediction model from Eq. (6), the reactance form is as follows:

$$\frac{X}{\rho_0 c_0} = X_m - f_X(U) - \cot(kh).$$

The first term represents mass reactance, and the second term represents incident wave effect. The third term represents the cavity reactance term. To expand the impedance prediction model to time-domain impedance model, the cavity reactance is changed into a polynomial form by applying a Laurent series. The trigonometric function of the cavity reactance would have a form of a series of odd functions of the polynomial function. That is, the polynomial form of the cavity reactance can be expanded like as follows:

$$\cot(kh) \cong \frac{1}{kh} - \frac{1}{3}(kh) - \frac{1}{45}(kh)^3 - \frac{2}{945}(kh)^5 + o(kh)^7. \tag{8}$$

Taking a wave number relation, $k = \left(\omega / c_0\right)$, the cavity reactance can be approximated by simple equation:

$$\cot(kh) \cong \frac{c_0}{\omega h} - \frac{1}{3}\left(\frac{\omega h}{c_0}\right). \tag{9}$$

Combining the mass reactance and the cavity reactance, the reactance of Eq. (6) is approximated by a polynomial form as follows:

$$\frac{X}{\rho_0 c_0} \cong X_m + \frac{1}{3}\left(\frac{\omega h}{c_0}\right) - \frac{c_0}{\omega h} - f_X(U). \tag{10a}$$

The coefficient X_m in Eq. (7) might be a first-order func-

tion or an arbitrary function with respect to ω by impedance prediction model. For GE impedance prediction model, X_m is first-order function, and X_m is easily changed into three parameter impedance model Eq. (3).

$$\frac{X}{\rho_0 c_0} \cong \frac{\omega(t+\varepsilon d)}{\sigma c_0} + \frac{1}{3}\left(\frac{\omega h}{c_0}\right) - \frac{c_0}{\omega h} - f_X(U) \tag{10b}$$

A resultant reactance term in the form of Eq. (3) can be determined from Eq. (10), and is given by

$$\frac{X}{\rho_0 c_0} = X_+ \omega + X_- \omega^{-1}. \tag{11}$$

The first term of the impedance model in Eq. (11) is linear relation with the angular frequency. Reactance coefficient X_+ is determined by the reactance relation of Eq. (10):

$$X_+ = \frac{t+\varepsilon d}{\sigma c_0} + \frac{1}{3}\left(\frac{h}{c_0}\right) - \left[0.119\frac{d}{\sigma c_0}\right]\cdot\log(U). \tag{12}$$

The reactance coefficient, X_- which shows the reverse relation with the angular frequency, is given by

$$X_- = -\frac{c_0}{h}. \tag{13}$$

Hence, three parameter impedance model in Eq. (3) can be re-written based on impedance re-construction model considering the incident intensity as follows:

$$\frac{Z}{\rho_0 c_0} = R_{GE} + f_R(U) - i\left[\left(\frac{t+\varepsilon d}{\sigma c_0} + \frac{1}{3}\left(\frac{h}{c_0}\right) - \left[0.119\frac{d}{\sigma c_0}\right]\cdot\log(U)\right)\omega - \frac{c_0}{h}\omega^{-1}\right]. \tag{14}$$

Hence, reconstructed TDIBC can be written by following form:

$$\frac{\partial v_n}{\partial t} = \frac{1}{X'_+}\left[p - R' v_n + X'_- V_n\right], \quad \frac{\partial V_n}{\partial t} = v_n \tag{15}$$

where

$$R' = R_{GE} + f_R(U),$$
$$X'_+ = \frac{t+\varepsilon d}{\sigma c_0} + \frac{1}{3}\left(\frac{h}{c_0}\right) - \left[0.119\frac{d}{\sigma c_0}\right]\cdot\log(U),$$

and $X'_- = -\frac{c_0}{h}$.

Tam and Auriault [4] provide a stability analysis for Eq. (15). To satisfy the stability condition for Eq. (15), impedance coefficients of Eq. (15) R', and X'_+ are real and positive. X'_- is to be real and negative. For case of extremely high level incident wave (U is more than 4.93), X'_+ is limited to $\frac{1}{c_0}\left(\frac{t}{\sigma}+\frac{h}{3}\right)$ [10]. Hence, all impedance coefficients satisfy the stability condition.

For the 6.7%-perforated-plate acoustic liner, the impedance measurement data are tabulated in Table 1 for cases overall sound pressure level (OASPL) 127 dB and 137 dB. In Table 2, we compare between impedance coefficients by mean-least-square fit [4] and impedance coefficients by Eq. (14). Fig. 2 shows the impedance curve for OASPL 127dB with experimental data. Impedance curve agrees well with impedance experimental data. Fig. 3 shows the impedance variation with respect to magnitude of incident wave and frequency.

Table 1. Impedance data sheet for 6.7 % perforate plate on frequency rages [1].

127dB

Frequency (Hz)	1100	1350	1750	2100	2450	2700	3000
Resistance [R]	0.13	0.14	0.19	0.25	0.25	0.21	0.2
Reactance [X]	-1.43	-0.94	-0.43	-0.07	0.21	0.44	0.71

137dB

Frequency (Hz)	1100	1350	1750	2100	2450	2700	3000
Resistance [R]	0.17	21	0.31	0.4	0.39	0.32	0.36
Reactance [X]	-1.46	-0.98	-0.48	-0.12	0.14	0.39	0.66

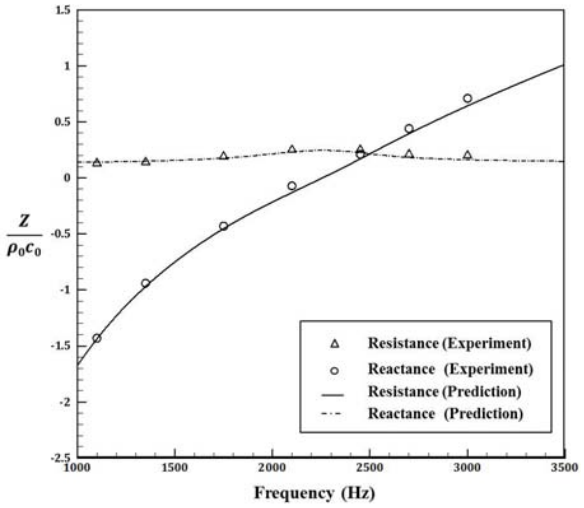

Fig. 2. Impedance curve comparison for 127 dB, △ : experimental resistance, ○ : experimental reactance [1], solid : predicted resistance, and, dash-dot : predicted reactance.

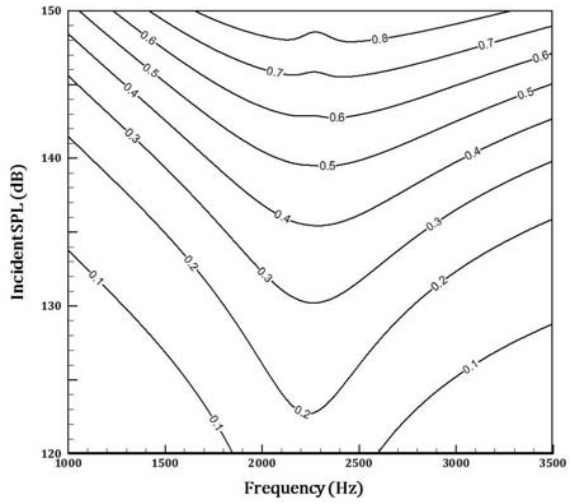

(a)

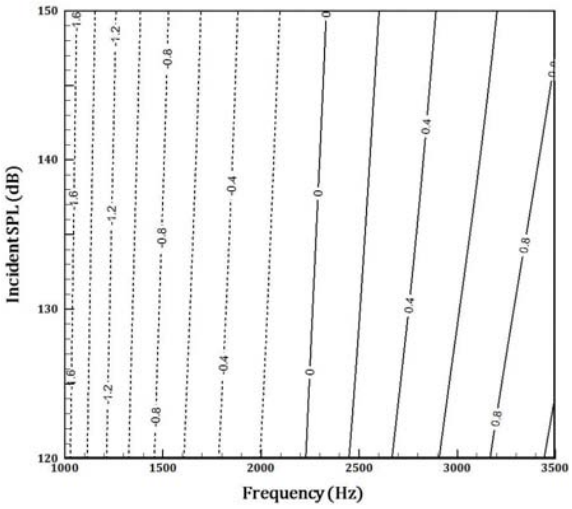

(b)

Fig. 3. Impedance map (incident SPL and frequency): (a) resistance; (b) reactance.

3.2 Determination process of magnitude of incident wave.

Time-domain impedance boundary condition (TDIBC) of Eq. (15) contains the magnitude of incident wave. The magnitude of incident wave of impedance is defined in frequency-domain as follows:

$$U = \sqrt{\sum_{i=1}^{n} \left(V_{rms,i}\right)^2} \tag{16}$$

$$V_{rms,i} = \frac{p_{rms,i}}{|Z_i|} \tag{17}$$

where $V_{rms,i}$ is the root-mean-square (RMS) value in the *i*-th frequency band. RMS value of $V_{rms,i}$ is coupled with local impedance Z_i and $p_{rms,i}$ in frequency-domain. To compute magnitude of incident wave, we consider a time-domain root-mean-square value of incident wave. In time-domain, magnitude of incident wave $U^{(n)}$ can be defined as

$$U^{(n)} = \sqrt{\frac{1}{T}\int_0^T v^2(t)\,dt}\ , \quad (T = n\Delta t) \tag{18a}$$

where $v(t)$ is time-domain signal.

Magnitude of incident wave $U^{(n)}$ can be characterized by

$$U^{(n)} = \sqrt{\left\{(n-1)\left[U^{(n-1)}\right]^2 + \left[v_n^{(n)}\right]^2\right\}\Big/ n}\ . \tag{18b}$$

Calculation of TDIBC of Eq. (15) and magnitude of incident wave $U^{(n)}$ is required an implicit calculation. To avoid implicit calculation, we introduce the temporal impedance with $U^{(temp)}$. In calculation of TDIBC of Eq. (15), we replace the $U^{(temp)}$ instead of $U^{(n)}$. Through calculation of TDIBC of Eq. (15), temporal magnitude of incident wave $U^{(temp)}$ is equal to $U^{(n-1)}$. Temporal values of acoustic pressure $p^{(temp)}$ and velocity $v_n^{(temp)}$ is obtained. Using temporal acoustic velocity $v_n^{(temp)}$, temporal magnitude of incident wave is iteratively updated by $U^{(temp)} = \sqrt{\left\{(n-1)\left[U^{(n-1)}\right]^2 + \left[v_n^{(temp)}\right]^2\right\}\Big/ n}$. Generally, iteration procedure converges quite rapidly. The detailed iteration procedure is shown Fig. 4.

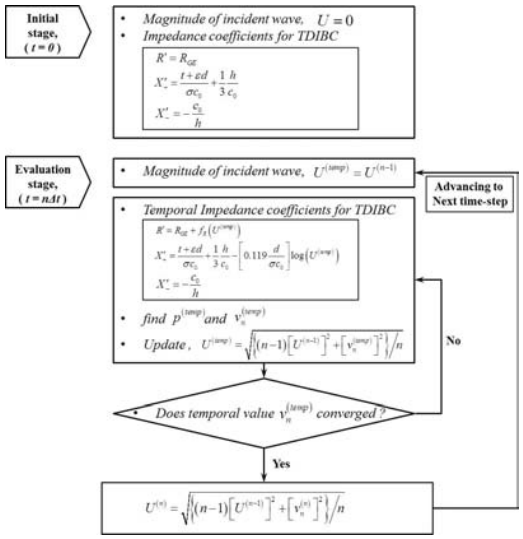

Fig. 4. Time-domain determination process of magnitude of incident wave.

4. Numerical evaluation

In order to evaluate the reconstructed TDIBC, two kinds of numerical computations are performed: (1) a one-dimensional wave propagation problem to account for the reflection wave that is relevant to the computation of impedance tube, and (2) acoustic field simulation of sound attenuation on impedance surface.

4.1 Numerical method and boundary conditions.

The equations of the acoustic field can be formulated by Linearized Euler equations (LEEs).

For the case of one-dimensional wave reflection problem, we simplify the LEEs by non-dimensionalization. LEEs can be described as follows:

$$\frac{\partial \mathbf{U}}{\partial t}+\frac{\partial \mathbf{E}}{\partial x}=0 \tag{19}$$

where $\mathbf{U}=\left[p \quad u\right]^{\mathbf{T}}$, and $\mathbf{E}=\left[u \quad p\right]^{\mathbf{T}}$.

For the case of acoustic field simulation, we consider the axisymmetric LEEs without mean-flow. The axisymmetric LEEs can be described as follows:

$$\frac{\partial \mathbf{U}}{\partial t}+\frac{\partial \mathbf{E}}{\partial x}+\frac{\partial \mathbf{F}}{\partial y}+\frac{1}{x}\mathbf{A}=\mathbf{S} \tag{20}$$

where

$$\mathbf{U}=\begin{bmatrix}\rho\\ u\\ v\\ p\end{bmatrix},\ \mathbf{E}=\begin{bmatrix}u\\ p\\ 0\\ u\end{bmatrix},\ \mathbf{F}=\begin{bmatrix}v\\ 0\\ p\\ v\end{bmatrix},\text{ and }\ \mathbf{A}=\begin{bmatrix}u\\ 0\\ 0\\ u\end{bmatrix}.$$

ρ represent the density perturbation, u and v are the velocity perturbation in the *x*- and *y*- directions, respectively. p is the pressure perturbation. $\mathbf{S}$ is the source vector and vector $\mathbf{A}$ is used in the axisymmetric problem. In this paper, density, velocity and pressure non-dimensionalized by ρ_0, c_0, and $\rho_0 c_0^2$. Coordinate system is scaled by the characteristic length L or H. The characteristic length of one-dimensional simulation is a tube length, L, and that of acoustic field simulation is a height of source position, H. Detailed information of numerical simulations is shown in Fig. 5.

In this work, the seven point dispersion-relation-preserving (DRP) scheme is selected for a discretization method of numerical calculation and the optimized 4th level Adams-Bashforth scheme is used for a time-integration [12].

For TDIBC condition, the reconstructed three parameter impedance boundary condition is used for impedance boundary condition. From Eq. (15), TDIBC is rewritten by a discrete form with time-step (n). By applying z-transform operator, $-i\omega \equiv \dfrac{\partial}{\partial t}=\dfrac{1-z^{-1}}{\Delta t}$ with time-derivative, the TDIBC can be derived by discrete form in time-domain. The resultant discretization form of Eq. (15) can be written as follows:

$$\frac{p^{(n+1)}-p^{(n)}}{\Delta t}=C_1\frac{v_n^{(n+1)}-v_n^{(n)}}{\Delta t}+C_2\frac{v_n^{(n-1)}}{\Delta t}+C_3\frac{v_n^{(n-2)}}{\Delta t}. \tag{21}$$

where $C_1=R'-X'_{-}\Delta t+X'_{+}/\Delta t$, $C_2=-\left(X'_{-}+X'_{+}/\Delta t^2\right)$,

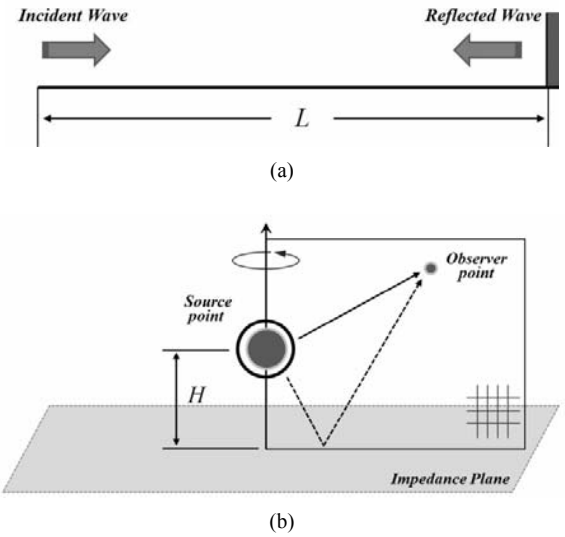

Fig. 5. Schematic view of numerical simulation: (a) normal incident impedance tube; (b) cylindrical coordinates system of wave reflection.

and $C_3=X'_{+}/\Delta t^2$.

Time discretization operator of flow quantity for Φ, $\left[\Phi^{(n+1)}-\Phi^{(n)}\right]/\Delta t$, can be expanded by 4th order Adams-Bashforth scheme. Finally, discretization form of Eq. (21) can be rewritten as follows:

$$\sum_{j=0}^{3}bj\left(\frac{\partial p}{\partial t}\right)^{n-j}=C_1\sum_{j=0}^{3}bj\left(\frac{\partial v_n}{\partial t}\right)^{n-j}+C_2\frac{v_n^{(n-1)}}{\Delta t}+C_3\frac{v_n^{(n-2)}}{\Delta t}. \tag{22}$$

4.2 One-dimensional wave reflection

We assume the wave reflection problem as a sum of harmonic waves with various incident magnitudes. In carrying out a reflection characteristic on an acoustical liner, the incident sound waves can be accounted as following form:

$$p_{incident}=\sum_{j=1}^{N}A_j\cos\left[\omega_j\left(x-t\right)\right] \tag{23}$$

where the variable A_j is the magnitude of the incident sound wave. Analytical solutions can be derived by the following form:

$$p(x,t)=\sum_{j=1}^{N}\left[A_j\exp\left(i\omega_j t-ik_j x\right)+A_j^{*}\exp\left(i\omega_j t+ik_j x+\varphi_j\right)\right]. \tag{24}$$

where φ_j and A_j^{*} can be written with impedance variable. R_j and X_j which is defined in impedance formula in frequency-domain of *j*-th harmonic excitation frequency.

$$\varphi_j=\tan^{-1}\left(\frac{2X_j}{R_j^2+X_j^2-1}\right), \tag{25a}$$

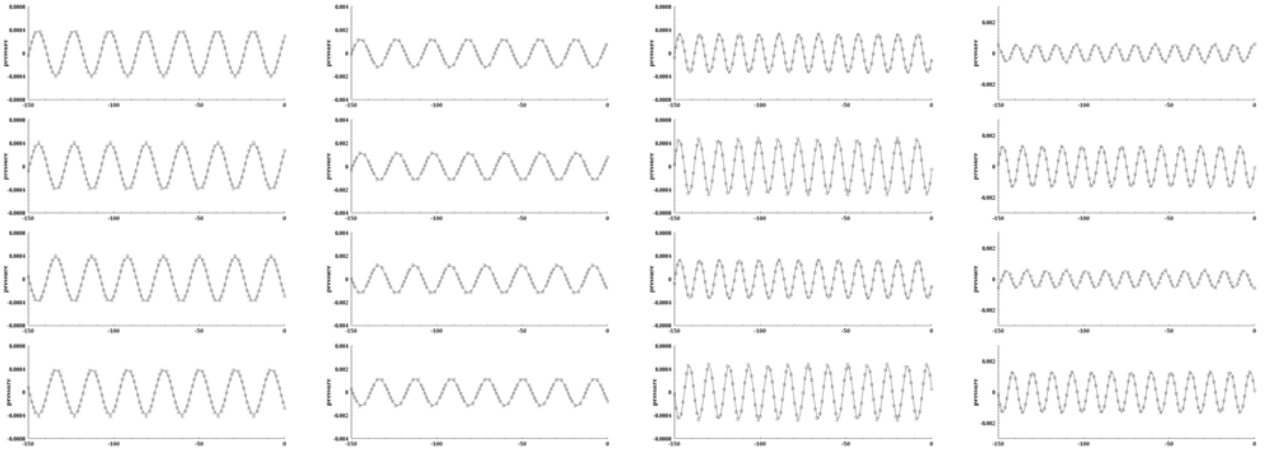

(a) (b) (c) (d)

Fig. 6. Numerical result comparison with $t = nT + 1/4T$, $t = nT + 1/2T$, $t = nT + 3/4T$ $t = nT$; ○ : analytical solution, and solid line : numerical simulation; (a) 1350 Hz, OASPL : 127 dB, (b) 1350 Hz, OASPL : 137 dB, (c) 2450 Hz, OASPL :127 dB, (d) 2450 Hz, OASPL :137 dB.

$$A_j^* = A_j = \frac{R_j - 1}{\left[\left(1 + R_j\right)\cos\varphi_j - X_j \sin\varphi_j\right]}. \tag{25b}$$

In numerical calculation, the incident wave boundary condition of Eq. (23) is applied on left side of impedance tube and the impedance boundary condition is applied on right side of impedance tube. We choose the uniform grid spacing with $\Delta x = L/150$. The numerical simulation is performed using a time step $\Delta t = 0.0001$. A one-dimensional wave propagation problem is divided by two problems: (1) single-frequency wave reflection with variant incident intensity and (2) quasi-broadband wave reflection problem of multiple excitation frequencies.

Case (1): Single-frequency wave reflection with variant incident intensity.

As mentioned before, a conventional TDIBC should be re-derived by the incident SPL condition. In order to show the capabilities of reconstructed TDIBC for variant incident wave condition, we calculate the single-frequency wave reflection problem. In numerical calculation, the excitation frequencies are 1350 Hz and 2450 Hz, and the magnitudes of incident sound wave are 127 dB and 137 dB over all sound pressure level (OASPL). For TDIBC, 6.7%-perforated-panel is chosen for an impedance boundary condition. For the incident sound wave with 127 dB OASPL, impedance quantities are $Z = \left(0.14 - 0.94i\right)$ and $Z = \left(0.25 + 0.21i\right)$ with 1350 Hz and 2450 Hz, respectively. For the incident sound wave with 137dB OASPL, the impedances are $Z = \left(0.21 - 0.98i\right)$ and $Z = \left(0.39 + 0.14i\right)$ with 1350 Hz and 2450 Hz, respectively.

Fig. 6 shows the comparison result between analytical solution and numerical solution. The numerical simulation is compared by the time-passage with $t = nT + 1/4T$, $t = nT + 1/2T$, $t = nT + 3/4T$ and $t = nT$. (T is period of incident sound wave). Numerical results agree well with analytical solutions.

Case (2): Quasi-broadband wave reflection with variant incident intensity.

In order to evaluate the broadband wave reflection, we choose a quasi-broadband wave with combination of multiple wave components. In numerical simulation, two wave components are used for a quasi-broadband wave source. One wave component is excited by 1350 Hz and its magnitude is 127 dB. The other is excited by 2450 Hz and its magnitude is 130 dB. To reconstruct the TDIBC condition, the magnitudes of wave components are summed. Finally, the OASPL of total sound wave is 131.76 dB. The surface impedance quantities for OASPL 131.76 dB can be obtained by GE impedance prediction model. The impedance quantities are $Z = \left(0.16 - 0.95i\right)$ for 1350 Hz and $Z = \left(0.31 + 0.18i\right)$ for 2450Hz.. The analytical sound field can be easily obtained by Eq. (24) through linear superposition.

Fig. 7 shows the comparison between numerical results and analytical results in quasi-broadband wave reflection simulation. The numerical result is shown by the time-passage with $t = 1850$, $t = 1900$, $t = 1950$ and $t = 2000$. (non-dimensional time). The time-domain results show the good agreement with summation of each analytical solution. It means that only one-time calculation is fully sufficient for multiple wave reflection. If *N* waves are propagating on an impedance surface, the numerical simulation which adopted the conventional impedance boundary conditions in the frequency domain should perform the *N*-times calculation. It is very convenient and reduces computation time especially in the broadband acoustic liner simulation.

4.3 Impedance surface wave reflection

In order to consider a wave reflection on an impedance surface, sound field due to broadband source is simulated. The

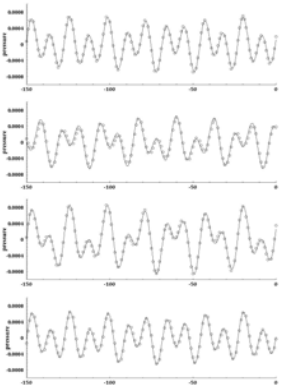

Fig. 7. Numerical result comparison of broadband wave with $t=1850$, $t=1900$, $t=1950$, and $t=2000$; ○ : analytical solution, and solid line : numerical simulation, wave-component 1 : 1350 Hz and 127 dB, wave-component 2 : 2450 Hz and 130 dB, OASPL : 131.76 dB.

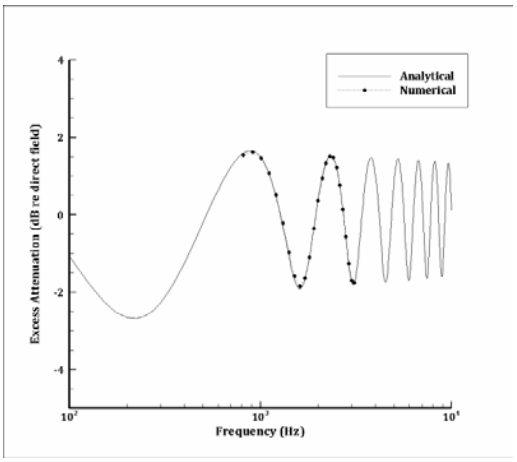

Fig. 8. Comparison of excess attenuation of sound due to monopole, • : numerical solution, and solid line : analytical solution.

sound filed is simulated in assumption of homogenous medium and without mean-flow. As shown in Fig. 5, the cylindrical coordinates is chosen for three-dimensional acoustic propagation, where x is the radial coordinate, y is the axial coordinate, and the impedance surface is located in $y=0$. The reconstructed TDIBC is applied on the impedance surface and radiation boundary condition is applied far-boundary condition.

In carrying out a sound field due to a broadband source, we choose the quasi-broadband source using summation of monopole sources as a source term in Eq. (20). In numerical simulation, a point source monopole is replaced by a Gaussian distributed monopole source to avoid the singularity of a point source monopole [13, 14].

$$f_m(r,t)=\frac{Amp}{B_w^3\pi^{3/2}}e^{-\left(r/B_w\right)^2+(kB_w)^2/4}\sin(\omega t) \tag{26}$$

where $r=|\vec{r}_s-\vec{r}_o|$ is a distance of the source at $\vec{r}_s$ and the observer $\vec{r}_o$, Amp represents the strength of Gaussian distributed monopole source, B_w is the half-width of a Gaussian distribution, and k is the wavenumber. The half pulse-width relative to the wavelength, $\overline{B}_w=B_w/\lambda$ used for a monopole source is quite small $\left(\overline{B}_w=3\times\Delta x\right)$ but enough to maintain a solution smoothness and to render an equivalent with a point monopole source. The broadband source can be obtained by a summation of Gaussian distributed monopole sources with variant angular frequency and source strength. Broadband source can be described as follows:

$$f_b(r,t)=\sum_{j=1}^{N}\frac{Amp_j}{B_w^3\pi^{3/2}}e^{-\left(r/B_w\right)^2+(kB_w)^2/4}\sin(\omega_j t) \tag{27}$$

where, $\omega_j=\omega_1+(j-1)\Delta\omega$ with $\omega_1=2\pi\times(800)$ and $\Delta\omega=2\pi\times(100)$, number of sources N is equal to 24. The incident intensity Amp_j is chosen by $120\,dB+(j-1)\times(0.5\,dB)$. In numerical simulation, broadband source is located on height of H from impedance surface, which H is the characteristic length with normalization.

Thus, the source position of this simulation is $(x_s,y_s)=(0,1)$. The numerical simulation is performed on a 200 by 300 equally spaced grid, whth spacing $\Delta x=\Delta y=1/80$. Numerical computations are performed using a time step of $\Delta t=CFL\times\Delta x$, where the Courant-Friedrichs-Lewy (CFL) number is 0.05.

To compare the numerical solution with analytical solution, an excess attenuation (EA) is calculated form an observer point, $(x_0,y_0)=(1,0.5)$. The wave reflection results are stored in time signals of source and observer point, and a fast Fourier transform (FFT) is used to obtain SPL in target frequency above described in Eq. (26).

Fig. 8 shows the numerical comparison of broadband reflection. The result of the excess attenuation of broadband impedance boundary condition has a good agreement with that of a summation of single wave reflection results. It represents that reconstructed impedance boundary condition has a good suitability in time-domain numerical computation, and variant incident intensity.

5. Concluding remarks

For a perforated-plate acoustic liner, a reconstruction method for time-domain impedance boundary condition (TDIBC) is proposed. Based on a GE impedance prediction model by Mostinger and Kraft, the coefficient of TDIBC is analyzed by geometric parameter of perforated-panel and re-derived using the frequency component and incident intensity component.

A determination process of impedance coefficients for reconstructed TDIBC is dependent on an impedance prediction model. This determination process is able to estimate the variation of impedance coefficients by incident magnitude of sound wave. In addition, this determination process is more useful to find impedance coefficients than other determination

process of conventional impedance boundary condition which is based on curve fitting method for impedance materials

The numerical simulation results of reconstructed TDIBC show a good agreement with the conventional impedance boundary conditions. The reconstructed TDIBC is able to simulate under the conditions of variant incident intensity.

The proposed reconstructed impedance boundary condition can be useful for varying incident pressure condition and an arbitrary acoustic liner. Using this impedance boundary condition in a numerical simulation, the noise reduction capability of a new acoustical treated panel can be evaluated for realistic conditions.

Acknowledgment

This work was supported by the Human Resources Development (No. 20094020100060) and the New and Renewable Energy Program (No.20104010100490) of the Korea Institute of Energy Technology Evaluation and Planning (KETEP) grant funded by the Korea government Ministry of Knowledge Economy.

Nomenclature

c_0 : Speed of sound
C_D : Discharging coefficient
R_0 : Resistance
X_m : Mass reactance
X_c : Cavity reactance
k : Wavenumber
σ : Porosity
Z : Acoustic impedance

References

[1] R. E. Mostinger and R. E. Kraft, Design and performance of duct acoustic treatment, *Aeroacoustics of Flight Vehicles : Theory and Practice*, NASA RP-1258 Aug. (1991) Chap. 14.

[2] K. J. Baumeister and E. J. Rice, *Visual study of the effect of grazing flow over an oscillatory flow in resonator orifice*, NASA TM X-3288, Sep. (1975).

[3] B. J. Tester, The propagation and attenuation of sound in lined ducts containing uniform and plug flow, *Journal of Sound and Vibration*, 28 (2) (1976) 151-203.

[4] C. K.W. Tam and L. Auriault, Time-domain impedance boundary conditions for computational aeroacoustics, *AIAA Journal*, 34 (5) (1996) 917-923.

[5] Y. Özyörük, L. N. Long and M. G. Jones, Time-domain numerical simulation of a flow impedance tube, *Journal of Computational Physics*, 146 (1) (1998) 29-57.

[6] S. W. Rienstra, Impedance models in time domain including the extended helmholtz resonator model, 12th AIAA/CEAS Aeroacoustics Conference, Cambridge, MA, 8-10 May (2006).

[7] K. Y. Fung and H. B. Ju., Broadband time-domain impedance model, *AIAA Journal*, 39 (8) (2001) 1449-1454.

[8] J. Bin, M. Y. Hussaini and S. Lee, Broadband impedance boundary conditions for the simulation of sound propagation in the time domain, *Journal of Acoustical Society of America*, 125 (2) (2009) 664-675.

[9] T. H. Melling, The acoustic impedance of perforates at medium and high sound pressure levels, *Journal of Sound and Vibration*, 29 (1) (1973) 1-65.

[10] R. E. Kraft, J. Yu, H. W. Kwan, B. Beer, A. F. Seybert and P. Tathavadekar, *Acoustic treatment design scaling methods: Phase II final report*, NASA-Langley Research Center: Hampton, VA, (2003).

[11] A. S. Hersh, B. E. Walker and J. W. Celano, Helmholtz resonator impedance model, Part 1 : Nonlinear Behavior *AIAA Journal*, 41 (5) (1999).

[12] C. K. W. Tam and J. C. Webb, Dispersion-relation-preserving finite difference schemes for computational aeroacoustics, *Journal of Computational Physics*, 107 (1993) 262-281.

[13] H. Ju and K. Fung, Time-domain simulation of acoustic sources over an impedance plane, *Journal of computational acoustics*, 10 (3) (2002) 311-329.

[14] X. Di and E. Gilbert, An exact Laplace transform formulation for a point source above a ground surface, *Journal of Acoustical Society of America*, 93 (2) (1993) 714-720.

[15] M. G. Jones, W. R. Watson and T. L. Parrott, Uncetainty and sensitivity analyses of a two-parameter impedance prediction model, 14th AIAA/CEAS Aeroacoustics, Monterey, VA. 2008.

[16] A. S. Hersh and B. Walker, Effect of grazing flow on acoustic impedance of Helmholtz resonators consisting of single and clustered orifices, F*inal Report Hersh Acoustical Engineering*, Aug. (1979).

[17] C. K.W. Tam, H. Ju and B. E. Walker, Numerical simulation of a slit resonator in a grazing flow, *44th AIAA Aerospace Sciences Meeting and Exhibit*, Reno, Nevada (2006).

[18]U. Ingard, H. Ising, Acoustic Nonlinearity of an Orifice, *Journal of Acoustical Society of America*, 42 (1) (1967) 6-17.

Minwoo Kim is a Ph.D. candidate in Mechanical and Aerospace Engineering at Seoul National University. He received his B.S. and M.S degrees in Mechanical and Aerospace Engineering from Seoul National University. His research interests are in the area of computational aeroacoustics.

Soogab Lee is a professor at the department of mechanical and aerospace engineering in Seoul National University. He received his Ph.D. degree in aeronautics and astronautics from Stanford University in 1992. He worked as a research scientist at NASA Ames Research Center from 1992 to 1995. His research interests are in the area of aerodynamics and acoustics of rotating machines including wind turbine systems.